Interpretation of variations in MODIS-measured greenness levels of Amazon forests during 2000 to 2009

2012 Environ. Res. Lett. 7 024018

(http://iopscience.iop.org/1748-9326/7/2/024018)

Environ. Res. Lett. **7** (2012) 024018 (12pp) doi:10.1088/1748-9326/7/2/024018

Interpretation of variations in MODIS-measured greenness levels of Amazon forests during 2000 to 2009

Arindam Samanta[1,2,6], **Sangram Ganguly**[3], **Eric Vermote**[4], **Ramakrishna R Nemani**[5] **and Ranga B Myneni**[1]

[1] Department of Geography and Environment, Boston University, Boston, MA 02215, USA
[2] Atmospheric and Environmental Research Incorporated, Lexington, MA 02421, USA
[3] BAERI/NASA Ames Research Center, Moffett Field, CA 94035, USA
[4] Department of Geography, University of Maryland, College Park, MD 20742, USA
[5] Biospheric Science Branch, NASA Ames Research Center, Moffett Field, CA 94035, USA

E-mail: arindam.sam@gmail.com

Received 20 February 2012
Accepted for publication 1 May 2012
Published 21 May 2012
Online at stacks.iop.org/ERL/7/024018

Abstract
This work investigates variations in satellite-measured greenness of Amazon forests using ten years of NASA Moderate Resolution Imaging Spectroradiometer (MODIS) enhanced vegetation index (EVI) data. Corruption of optical remote sensing data with clouds and aerosols is prevalent in this region; filtering corrupted data causes spatial sampling constraints, as well as reducing the record length, which introduces large biases in estimates of greenness anomalies. The EVI data, analyzed in multiple ways and taking into account EVI accuracy, consistently show a pattern of negligible changes in the greenness levels of forests both in the area affected by drought in 2005 and outside it. Small random patches of anomalous greening and browning—especially prominent in 2009—appear in all ten years, irrespective of contemporaneous variations in precipitation, but with no persistence over time. The fact that over 90% of the EVI anomalies are insignificantly small—within the envelope of error (95% confidence interval) in EVI—warrants cautious interpretation of these results: there were no changes in the greenness of these forests, or if there were changes, the EVI data failed to capture these either because the constituent reflectances were saturated or the moderate resolution precluded viewing small-scale variations. This suggests a need for more accurate and spatially resolved synoptic views from satellite data and corroborating comprehensive ground sampling to understand the greenness dynamics of these forests.

Keywords: Amazon, greenness, remote sensing

1. Introduction

Quantifying variations in the greenness of Amazonian forests and understanding the driving factors behind these variations is an important research theme considering the role these forests play in the global carbon (Malhi and Grace 2000) and hydrological cycles (e.g., McGuffie *et al* 1995, Werth and Avissar 2002). This remains a challenging task for investigation through ground sampling, given the sheer expanse of these forests, 5.3 million km^2, with most of it presently inaccessible (Aragao *et al* 2009), and enormous heterogeneity and rich biodiversity (e.g., Phillips *et al* 1994, ter Steege *et al* 2006). Satellite greenness data—NASA moderate resolution imaging spectroradiometer (MODIS) enhanced vegetation index (EVI) data (Justice *et al* 1998,

[6] Address for correspondence: Atmospheric and Environmental Research Incorporated, 131 Hartwell Avenue, Lexington, MA 02421, USA.

Vermote *et al* 2002, Huete *et al* 2002)—provide repetitive synoptic sampling of the entire Amazon basin, albeit at a moderate resolution. Algorithm refinements through feedback from concerted validation efforts and multiple reprocessings of the growing MODIS data archive have led to progressively improved research-quality products ideally suited for studies of greenness dynamics in complex ecosystems such as the Amazon (e.g., Huete *et al* 2006, Xiao *et al* 2006, Myneni *et al* 2007, Samanta *et al* 2011b, 2012, Xu *et al* 2011). A particularly appealing aspect of these data is their record length—presently over a decade. Therefore, these data are potentially well suited to research variations in greenness levels across this wide basin.

Investigation of greenness dynamics with satellite measurements is fraught with several pitfalls, the major being corruption from atmospheric effects leading to artificial changes in vegetation indices that are unrelated to any real changes on the ground. This is especially true of the Amazon, where clouds and aerosols from biomass burning are seemingly ubiquitous. For example, Saleska *et al* (2007) observed a greening anomaly in response to the 2005 drought, but this was shown to be an artifact of atmospheric corruption of EVI and not observed in a later version of the same data (Samanta *et al* 2010, 2011a). Similarly, corruption of satellite data was also recently found to be a key issue in the lack of reliability of vegetation growth trends reported by Zhao and Running (2010), especially in the Amazon (Samanta *et al* 2011b). Thus, the motivation for this work derives from the recurring theme of data contamination impacts on interpretation of variations in vegetation activity in the Amazon, which has not only been reported for singular events such as the 2005 drought (Samanta *et al* 2010, 2011a), but also, more recently, for vegetation growth trends (e.g., Samanta *et al* 2011b). Bearing this in mind and with a view to informing future studies, we have presented a number of new analyses and results. First, estimates of biases resulting from screening corrupted data from analysis. Second, analysis of characteristics of greenness dynamics, taking into consideration the statistical distributions of measurement errors of the greenness data. Third, further investigation of relationship between greenness and precipitation anomalies. Fourth, investigation of persistence of greenness changes over time.

2. Data

2.1. Vegetation greenness data

Enhanced vegetation index (EVI) is a satellite data based measurement of vegetation greenness produced by NASA using blue (459–479 nanometers (nm)), red (620–670 nm) and near-infrared (842–876 nm) band surface reflectance data from the MODIS instrument aboard the Terra and Aqua satellites (WWW1 2011, Huete *et al* 2002). EVI generally correlates well with ground measurements of photosynthesis (e.g., Rahman *et al* 2005, Sims 2008) and is found to be especially useful in high biomass tropical broadleaf forests like the Amazon (Huete *et al* 2006). We used versions—also called Collections—4 and 5 of Terra MODIS EVI data. Collection 5 (C5) is the latest version, superseding all previous versions.

The dataset 'Vegetation Indices 16-Day L3 Global 1 km'—MOD13A2—contains EVI at 1×1 km^2 spatial resolution and 16-day frequency. This 16-day frequency arises from compositing, i.e. assigning one best-quality EVI value to represent a 16-day period. This dataset is available in tiles (10°$\times$ 10°at the equator) of sinusoidal projection—16 such tiles cover the Amazon region (approximately 10°N–20°S and 80°W–45°W). The data were obtained from the NASA Land Processes Data Active Archive Center (LP DAAC) (WWW1 2011) for the period February 2000–December 2009. A previous version of EVI data, Collection 4 (C4), was also used in this study, although this dataset is now decommissioned and deleted from the NASA LPDAAC archives (the July to September C4 Terra MODIS EVI data, but not the corresponding quality flags, for the years 2000–5, were obtained from Saleska *et al* (2007)). We have also used two other datasets. First, we used the dataset 'Vegetation Indices Monthly L3 Global 0.05° CMG'—MOD13C2—which contains EVI at 0.05°$\times$0.05° spatial resolution and monthly frequency. Second, we used the dataset 'Vegetation Indices 16-Day L3 Global 0.05° CMG'—MOD13C1—which contains EVI at 0.05°$\times$0.05° spatial resolution and 16-day frequency. These are 'cloud-free spatial composites' of MOD13A2 (WWW2 2011). These were obtained from the NASA LP DAAC (WWW2 2011) for the period February 2000–December 2009. We also were able to obtain C4 MOD13C1 data with quality flags for 2004–6 (WWW2 2011).

2.2. Land cover data

Land cover information was obtained from the 'MODIS Terra Land Cover Type Yearly L3 Global 1 km SIN Grid' product—MOD12Q1. This is the official NASA C5 land cover data set (WWW3 2011, Friedl *et al* 2010). It consists of five land cover classification schemes at 0.5×0.5 km^2 spatial resolution. The International Geosphere Biosphere Programme (IGBP) land cover classification scheme was used to identify forest pixels in the Amazon region.

2.3. Precipitation data

The dataset 'Tropical Rainfall Measuring Mission (TRMM) and Other Data'—3B43—consists of monthly precipitation rate (mm h^{-1}) at 0.25° $\times$ 0.25° spatial resolution (WWW4 2011). This dataset covers the region 50°N–50°S and 180°W–180°E. We used the latest version (version6) spanning July to September of years 1998–2009 in this study.

3. Methods

3.1. Determination of EVI validity

The presence of clouds (adjacent clouds, mixed clouds and shadows) 'obscures' the surface in a radiometric sense, thus corrupting inferred EVI values. In addition, two types of

aerosol loadings typically corrupt EVI—climatology and high aerosols. Use of aerosol climatology indicates that the actual aerosol content is unknown, most likely due to the presence of clouds, and aerosol correction was performed using historical or climatological aerosol optical thickness (AOT) data (Vermote and Vermuelen 1999). Moreover, atmospheric correction methods are ineffective for high aerosol loadings (AOT > 0.5) (WWW5 2011, WWW6 2011, Didan and Huete 2006), especially in the shorter red and blue spectral bands (Vermote and Kotchenova 2008) used by EVI (Huete *et al* 2002).

Each 1×1 km^2 16-day composite EVI value is considered valid when (a) EVI data is produced—'MODLAND_QA' equals 0 (good quality) or 1 (check other QA), (b) VI usefulness is between 0 and 11, (c) clouds are absent—'adjacent cloud detected' (0), 'mixed clouds' (0) and 'possible shadow' (0), and (d) aerosol content is low or average—'aerosol quantity' (1 or 2). Note that 'MODLAND_QA' checks whether EVI is produced or not, and if produced, its quality is good or whether other quality flags should also be checked. Besides, VI usefulness indices between 0 to 11 essentially include all EVI data. Thus, these two conditions serve as additional checks.

Each $0.05° \times 0.05°$ 16-day/monthly EVI pixel is considered valid when (a) EVI data is produced—'MODLAND_QA' equals 0 (good quality) or 1 (check other QA), (b) VI usefulness is between 0 and 11, (c) clouds are absent—'adjacent cloud detected' (0) and 'mixed clouds' (0), (d) aerosol content is low or average—'aerosol quantity' (1 or 2), and (e) consistency with finer resolution EVI—'geospatial quality' ($\geq$50%). Here, the utility of 'MODLAND_QA' and VI usefulness flags is same as in the case of 1×1 km^2 EVI validity. Besides, the 'geospatial quality' flag provides information on the fraction of 1×1 km^2 EVI data that contributed to each $0.05° \times 0.05°$ EVI pixel.

3.2. Evaluation of EVI standardized anomalies

Standardized anomalies (anomaly divided by the standard deviation) are calculated pixel-by-pixel for the dry season in central and southern Amazon, July to September—the third quarter of a year. These anomalies may be calculated using two different methods.

3.2.1. Method of equal record lengths. The dry season in a calendar year spans six 16-day EVI composites—numbered 177 through 257. Of these, two consecutive composites cover each month—July (177 and 193), August (209 and 225) and September (241 and 257). For each month, if both the 16-day EVI values are valid, the average of the two is the monthly value. If only one of the two is a valid EVI value, it represents the monthly value. If none are valid EVI values, the monthly mean does not exist and the pixel is not used in further calculations. For each year, if all three EVI monthly values exist, these are averaged to obtain the third-quarter mean, else the quarterly mean does not exist. If the quarterly mean EVI exists in all years of a reference period, the mean ($\mathrm{EVI}^{\mathrm{JAS}}_{\mathrm{mean,ref}}$) and standard deviation ($\sigma^{\mathrm{JAS}}_{\mathrm{ref}}$) are evaluated. The reference period is generally 2000–6 (excluding 2005) for C5 EVI and 2000–4 for C4 EVI, unless stated otherwise. Finally, if the 2005 quarterly mean EVI exists, the standardized anomaly is calculated as:

$$\mathrm{EVI}^{\mathrm{JAS}}_{\mathrm{stn\_anom,2005}} = \frac{\mathrm{EVI}^{\mathrm{JAS}}_{\mathrm{mean,2005}} - \mathrm{EVI}^{\mathrm{JAS}}_{\mathrm{mean,ref}}}{\sigma^{\mathrm{JAS}}_{\mathrm{ref}}}. \qquad (1)$$

This method minimizes biases in the evaluation of standardized anomalies because it is based on equal record lengths for all pixels. However, this method increases the time step from 16 days to a month and pixels with atmosphere-corrupted data are dropped from all further analysis. This method was used in Samanta *et al* (2010).

3.2.2. Method of unequal record lengths. For each year, the quarterly mean EVI is calculated as the average of all available 16-day composite EVI values, after screening for clouds and aerosols. Following this, $\mathrm{EVI}^{\mathrm{JAS}}_{\mathrm{mean,ref}}$ and of the reference period are evaluated from all available dry season mean EVI values. The 2005 EVI standardized anomalies are then calculated using the expression in (1). The lengths of EVI data record used to evaluate these quantities vary from pixel-to-pixel, because this method does not require that all months have a valid EVI value, which introduces biases in the anomaly estimates (cf the appendix). This method was used in Saleska *et al* (2007).

3.3. Evaluation of precipitation ($0.25° \times 0.25°$) standardized anomaly

A monthly precipitation value is considered 'valid' if it is not equal to -9999. If all the three monthly precipitation values are valid, the total of the three represents the quarterly total. Else, the pixel is tagged and not used in further calculations. The rest of the processing is similar to that described in section 3.2.1. The reference period for precipitation is generally 1998–2006 (excluding 2005), unless stated otherwise. Pixels with precipitation standardized anomalies less than -1 std. dev. are classified as drought-stricken (Saleska *et al* 2007, Samanta *et al* 2010).

4. Results and discussion

4.1. Greenness dynamics during the 2005 drought

Atmosphere-corrupted EVI data should be filtered from analysis to reliably study vegetation greenness dynamics due to two reasons—first, EVI changes significantly during the course of a given year (figure 1(a)). Second, contamination of data with clouds and aerosols is prevalent in this region (Samanta *et al* 2010, 2011a)—even in the dry season 60–66% of these data are corrupted with atmospheric effects (figure 1(b)). The filtering can be done either with the quality flags or the VI Usefulness Indices accompanying the EVI data. This not only reduces the number of EVI data available for analysis, but also poses a problem when evaluating EVI statistics such as temporal means, standard

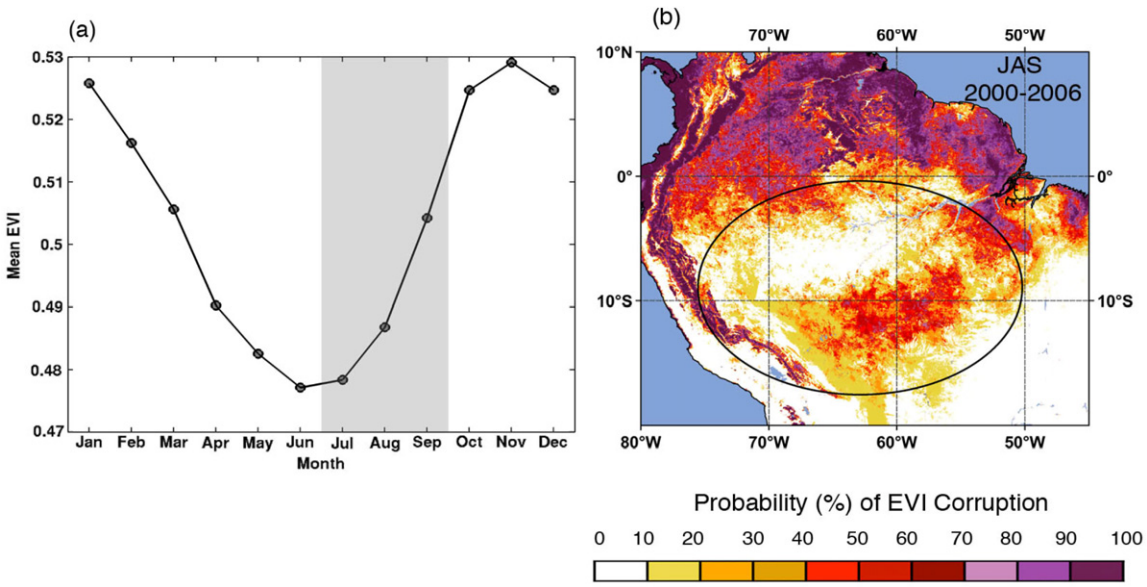

Figure 1. (a) Annual course of monthly C5 EVI (0.25° × 0.25°), averaged over Amazon forests in the region covering 0°–23.5° S and 80°–45°W, for the period 2000–6. EVI data are screened for clouds (adjacent and mixed clouds and cloud shadows) and aerosols (high and climatology aerosols). (b) Spatial patterns of the probability (%) of EVI (1 × 1 km^2) corruption during July to September (JAS) quarter. A 16-day composite C5 EVI value is valid when its quality flags indicate absence of clouds (adjacent clouds, mixed clouds and possible shadows) and aerosols (climatology and high). If at least one 16-day composite is valid in a month, then the monthly EVI is valid. Similarly, if all three months in a quarter have valid EVI, then the quarterly EVI is valid and the 1 × 1 km^2 pixel is given a validity score of 1. Thus, for each quarter during the 2000–6 time period, a pixel can have a maximum cumulative validity score of 7. Then, the probability (%) of validity of a pixel is calculated as (100(cumulative validity)/(maximum cumulative validity)). Finally, the probability (%) of corruption of the pixel is calculated as (100-probability of validity).

deviations and anomalies. Consider, for example, the July to September quarterly standardized anomaly (a) in year 2005. It is evaluated as $(x - m)/s$, where x is the quarterly mean in year 2005, m is the climatological quarterly mean and s is the corresponding quarterly standard deviation. The unbiased evaluation of these quantities requires the complete set of 16-day EVI composite data over a long enough time period for each pixel in the study area. Filtering atmosphere-corrupted EVI data makes this set incomplete. Thus, the EVI record lengths will vary from pixel-to-pixel across the study region. The evaluation of x, m, s and a under these circumstances (cf section 3.2.2) introduces large biases for two reasons—large increase in EVI during the July to September quarter (figure 1(a)), (Huete *et al* 2006, Samanta *et al* 2012) and short record lengths (less than 10 yr). These biases are quantified in appendix—they can be minimized by requiring that every month has at least one uncorrupted EVI value (cf section 3.2.1). Even then, a large number of pixels will not have the requisite record length and should therefore be dropped from analysis. We used both these methods—unequal record lengths at 16-day scale and equal record lengths at monthly scale—to characterize the spatial patterns of greenness dynamics in the drought-affected region of the Amazon. To filter the corrupted data, we used Collection 5 (C5) data quality filters for both C4 and C5 EVI data (cf section 3.2). This facilitated a more accurate assessment of atmosphere-corruption effects across Collections by not introducing errors related to changes in data filters between collections.

4.1.1. Method of unequal record lengths. Changes in EVI spatial patterns resulting from successive filtering of cloud- and aerosol-contaminated data with quality flags are shown in figure 2, and numerically tabulated in table 1. Pixels with EVI standardized anomalies greater than +1 are categorized as greening, less than −1 as browning, and between −1 and +1 as displaying no changes (Saleska *et al* 2007, Samanta *et al* 2010). The unfiltered C4 and C5 patterns are very different (figures 2(a) and (b))—three prominent patches of greening seen in C4, of which one is very large (approximately 300 000 km^2), are missing in C5. The extent of greening decreases (11%) and browning increases (8%) in C5 compared to C4. The dominant pattern in both EVI collections is one of no EVI changes (51–54%). Screening for clouds and their shadows minimally changes the respective patterns in both collections (less than 7%) (figures 2(c) and (d)). However, screening for high aerosol amount significantly reduces the greening (by 34%) and enhances the browning extents in C4 (by 55%), but not in C5 (figures 2(e) and (f)). Overall, filtering of atmosphere-corrupted EVI data reduces the anomalous greening proportion by 36% and enhances the browning proportion by 65% in C4. The final patterns, after both cloud and aerosol screening, are similar across collections—the dominant pattern, spanning 57% of the drought-affected area, remains one of no EVI changes, the rest exhibiting anomalous greening and browning patterns (25% and 18%) (table 1).

Another way to filter pixels for dataquality is by using VI usefulness indices. Index values 4 and above generally

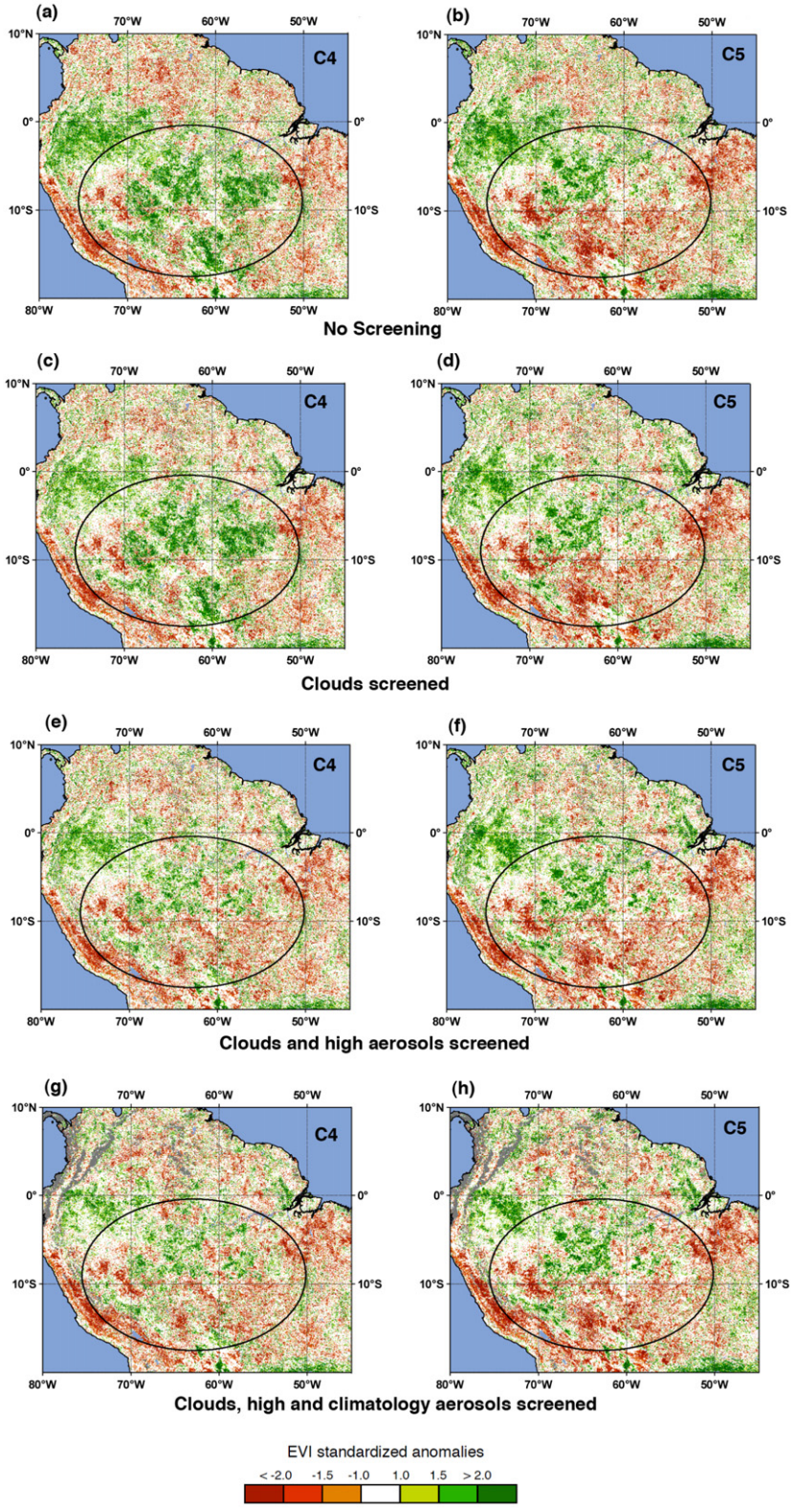

Figure 2. Spatial patterns of EVI standardized anomalies during the 2005 dry season (July–September) at 1×1 km^2 spatial resolution. Panels (a) and (b) show patterns when no data are screened. Panels (c) and (d) show patterns when cloud-contaminated (adjacent cloud, mixed clouds and cloud shadows) data are screened. Panels (e) and (f) show patterns when cloud- and high aerosol-contaminated data are screened. Panels (g) and (h) show patterns when cloud- high aerosol- and climatology aerosol-contaminated pixels are screened. C4 and C5 refer to collection 4 and 5 EVI data sets. For consistency between C4 and C5 EVI, anomalies are calculated relative to 2000–4, using the methodology described in section 3.2.2. The ellipse in the panels shows the drought-affected region.

Table 1. Effect of data filtering on collections 4 (C4) and 5 (C5) EVI (1 × 1 km^2) standardized anomalies during the dry season, July to September, of year 2005. Pixels with EVI standardized anomalies in the range −1 to +1 standard deviation (std. dev.) are classified as showing no changes. Pixels with EVI standardized anomalies less than −1 std. dev. are classified as browning. Pixels with EVI standardized anomalies greater than +1 std. dev. are classified as greening. Shown here are changes in fractions (%) of greening (Δ greening), browning (Δ browning) and 'no-change' (Δ no change) in drought-stricken forests, south of the equator, when EVI data are screened using quality flags pertaining to clouds and aerosols (figure 2) as well as VI usefulness, relative to no data screening.

		Δ greening (%)		Δ browning (%)		Δ no change (%)	
Screening type	Cumulative screening	C4	C5	C4	C5	C4	C5
Quality flags	No screening	0	0	0	0	0	0
	Adjacent clouds	−4.18	−2.12	3.16	0.59	2.41	0.81
	Mixed clouds	−5.44	−3.47	5.21	1.35	2.92	1.23
	Cloud shadows	−6.23	−7.67	3.10	3.46	3.62	2.34
	High aerosols	−33.56	−5.41	55.25	−2.22	12.63	2.73
	Climatology aerosols	−35.97	−9.61	65.12	0.43	11.57	2.62
VI usefulness index	VI usefulness >4 screened	−5.63	−6.18	4.65	2.54	3.10	2.10
	VI usefulness >3 screened	−34.22	−6.43	59.25	−1.20	12.24	2.82
	VI usefulness >2 screened	−40.37	−18.45	62.42	−0.11	14.22	6.67

correspond to pixels with atmosphere-corrupted EVI values and conversely, indices three and below correspond to uncorrupted EVI values. The changes in EVI spatial patterns resulting from screening with these indices are similar to those with quality flags (table 1). Inclusion of atmosphere-corrupted EVI values results in very different patterns between C4 and C5 (figure not shown for brevity)—again, three prominent C4 greening patches are missing in C5. The greening proportion decreases (by 28.77%) and browning proportion increases (by 68.53%) in C5 compared to C4, but the dominant proportion of pixels in both collections still shows no EVI changes (53–55%). Screening for clouds and aerosols, that is, using indices less than 4, results in similar patterns across the two collections (figure not shown for brevity)—again, the dominant pattern is one of no EVI changes (56–57%). This analysis is consistent with screening by quality flags (figure 2). Together these results indicate that atmosphere-corrupted EVI values are comparable to uncorrupted values in C5, but are large over-estimates in C4. Therefore, the C4 patterns, in the absence of any data quality filtering, or only cloud filtering, are artifacts of atmospheric effects on EVI. Note that atmosphere-corrupted pixels may be inadvertently included in the analysis either by ignoring the quality flags or if the quality flags are faulty, that is, the atmosphere-corrupted pixels are tagged as uncorrupted. The fact that the results published in Saleska *et al* (2007) match our C4 patterns without any data quality filtering (figure 2(a)) and with cloud filtering only (figure 2(c)) indicates (inadvertent) inclusion of aerosol-corrupted EVI data in their analysis. Moreover, the results presented in this section should be interpreted with caution for two reasons—first, the evaluation of standardized anomalies without regard to the availability of the full complement of EVI data introduces biases depending on the remaining record lengths (cf appendix), and second, the use of ±1 standardized deviation alone to categorize greenness dynamics does not account for the statistical significance of observed EVI changes, as discussed in section 4.1.2.

4.1.2. Method of equal record lengths. The quarterly standardized anomalies are evaluated only for pixels without atmosphere-corrupted monthly EVI data, as in Samanta *et al* (2010) (cf section 3.2.1). Of the nearly 2.19 million km^2 of intact Amazon forests in the drought-stricken region, 12% (0.26 million km^2) show anomalous greening (EVI std. anomalies greater than +1), 6% (0.13 million km^2) show browning (EVI std. anomalies less than −1) and 22% (0.48 million km^2) show no EVI changes (EVI std. anomalies between −1 and +1)—the rest, 60% (1.32 million km^2), have atmosphere-corrupted EVI data, and are therefore excluded from further analysis (figure 3(a)). It is prudent to explore whether the area with uncorrupted EVI data (40%) is representative of the entire drought-affected region. If so, the EVI dynamics may be expressed relative to the area of valid data, in which case, the greening and browning proportions increase to 30% and 15%, respectively. The dominant pattern, nevertheless, remains one of no greenness changes (55%). We argue that the area sampled is not representative of the larger drought-affected region, that is, the sample of pixels with uncorrupted EVI data is not representative of the total population of pixels in the drought region, for the following reasons.

Atmosphere-corruption of EVI data due to clouds and aerosols is highly selective, both spatially and temporally (cf figure 1(b)). The broad precipitation gradient in the Amazon, and its seasonal variations, from the less humid southeast to the more humid northwest (Sombroek 2001) implies a similar gradient in cloud persistence—therefore, the probability of obtaining cloud-free satellite data in the more humid forests is selectively lower. Aerosols from biomass burning are predominant in the southeastern fringes in the dry season—for example, figure 3 in Aragao *et al* (2007)—therefore, the probability of EVI corruption from aerosols is selectively higher in these areas during the dry season, and nearly non-existent in other seasons (April to June, for example). Thus, forests to the northwest and southeast will be under-sampled and forests to the center will be over-sampled—figure 1(b) (similar patterns for other

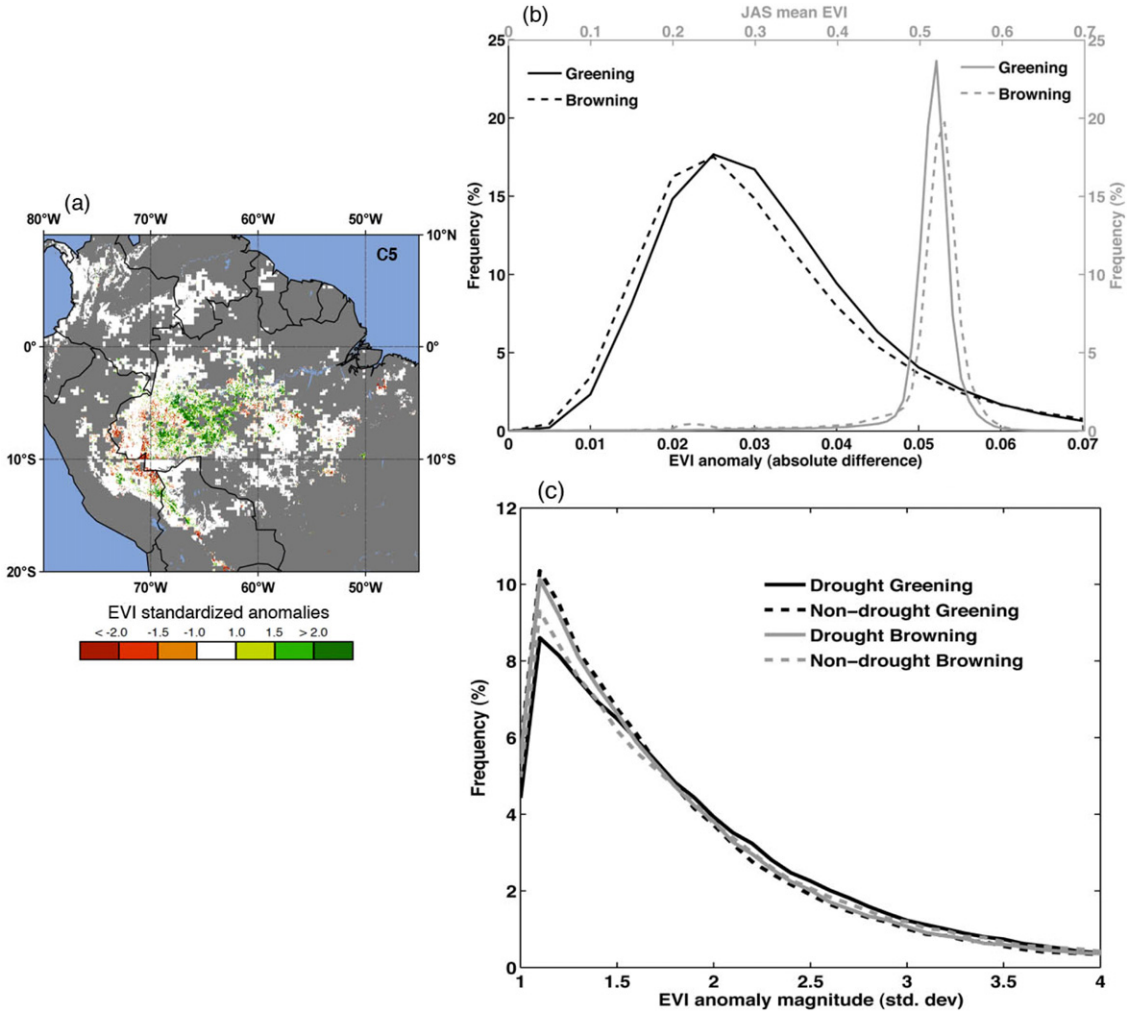

Figure 3. (a) Spatial patterns of collection 5 (C5) EVI standardized anomalies during the 2005 dry season (July to September, JAS) at 1×1 km^2 spatial resolution. Cloud-, shadow-, climatology aerosol- and high aerosol-contaminated data are screened from analysis. Anomalies are calculated relative to 2000–6, but excluding 2005. (b) Frequency distribution (%) of 2005 dry season EVI standardized anomalies, expressed as absolute (EVI) difference, and dry season mean EVI averaged over 2000–6 (excluding 2005) for forests displaying greening (JAS EVI standardized anomaly $>$ 1 std. dev.) and browning (JAS EVI standardized anomaly <-1 std. dev.). (c) Frequency distribution (%) of dry season EVI standardized anomalies for drought-impacted and non-impacted forests south of the equator exhibiting greening and browning.

quarters not shown for brevity). Given the rich diversity of species and their varied responses to variations in climate, this biased sampling argues against extrapolating the uncorrupted data available for the smaller area to the much larger drought-affected region.

The area with uncorrupted EVI data increases to 65–75% of the drought-affected region, if the analysis is performed on monthly, rather than quarterly, standardized anomalies. Nevertheless, a predominant proportion (60–65%) still shows no anomalous EVI changes in each of the three months of the dry season, consistent with the analysis on quarterly standardized anomalies.

In fact, the use of a threshold value of standardized anomaly ($\pm$1 std. dev.) alone to categorize greenness dynamics, without an account of the magnitude (absolute value) of EVI changes, relative to EVI accuracy, is misleading, for it does indicate whether the observed anomalies are real or not. For instance, the 60% of all EVI anomalies that are within 0.02 EVI in magnitude may be considered insignificant, because the 1 std. dev. envelope of error in EVI is $\pm$(0.02 + 2% of EVI) (Vermote and Kotchenova 2008). Similarly, 97% of the EVI anomalies in greening and 94% in browning categories fall within the 2 std. dev. (95% confidence interval) envelope of error in EVI ($\pm$0.06, which is about 12% of the climatological dry season average EVI value of 0.51) (figure 3(b)). Therefore, over 90% of the EVI anomalies are insignificantly small i.e. within 2 std. dev. representing the 95% confidence interval of error in EVI, which is about $\pm$0.06 or 12% of the dry season average EVI value of 0.51. Thus, using a threshold of 12% EVI change, in addition to 1 std. dev., to categorize EVI dynamics reduces the anomalous greening and browning proportions to 0.6% and 0.5%, respectively. This further re-enforces the dominant greenness dynamic as one of no changes during the dry season drought of 2005. The fact that a majority of the measured EVI anomalies are insignificantly small could suggest either

Table 2. Changes in collection 5 (C5) EVI (1 × 1 km^2) and precipitation (0.25°×0.25°) during dry seasons (July to September, JAS) of years 2000–9. Only forest pixels, in the region 0° to 20°S and 45°W to 80°W, located in areas with JAS 2005 precipitation anomaly less than −1 std. dev. (relative to the mean for the 1998–2006 period, excluding 2005) are considered. The EVI standardized anomalies are relative to the mean for the 2000–9 period. The precipitation standardized anomalies are relative to the mean for the 1998–2009 period. In both cases, year 2005 data are excluded. Pixels with EVI standardized anomalies in the range −1 to +1 std. dev. are classified as showing no changes. Pixels with EVI standardized anomalies less than −1 std. dev. are classified as browning. Pixels with EVI standardized anomalies greater than +1 std. dev. are classified as greening. Pixels with precipitation standardized anomalies less than −1 std. dev. are categorized as drought-stricken or with precipitation deficit. Cloud-, shadow-, climatology aerosol- and high aerosol-contaminated data are excluded from analysis.

Year	Precipitation deficit area (%)	Greening (%) (magnitude (std))	Browning (%) (magnitude (std))	No change (%)	Valid pixels (%)
2000	1.27	5.72 (1.38)	4.63 (−1.41)	23.95	34.32
2001	5.65	5.64 (1.38)	5.72 (−1.43)	24.03	34.32
2002	9.20	5.59 (1.39)	4.71 (−1.42)	24.01	34.32
2003	5.23	8.74 (1.44)	3.20 (−1.41)	22.38	34.32
2004	5.06	8.08 (1.47)	5.53 (−1.49)	20.69	34.32
2005	86.25	11.19 (1.84)	3.16 (−1.67)	18.59	32.95
2006	26.15	5.42 (1.35)	2.83 (−1.36)	26.06	34.32
2007	40.83	5.20 (1.38)	5.04 (−1.4)	24.07	34.32
2008	18.36	3.29 (1.34)	4.73 (−1.37)	26.29	34.32
2009	16.02	0.79 (1.34)	14.99 (−1.50)	18.53	34.32

reflectance saturation in dense Amazon canopies or no real changes in the greenness of these forests.

It is also of interest to contrast the greenness dynamics of forests within the drought-affected region to forests outside this region, but south of the equator. Of the nearly 2.44 million km^2 of such forests, about 5% (0.12 million km^2) show anomalous greening, 5% (0.12 million km^2) show browning and 14% (0.34 million km^2) show no EVI changes—the rest, 76% (1.86 million km^2), have atmosphere-corrupted data and are therefore excluded from analysis. Nearly 93% of these forests with uncorrupted data have EVI anomalies that fall within the 2 std. dev. (95% confidence interval) envelope of error in EVI. Thus, as before, using a threshold of 12% EVI change, in addition to 1 std. dev., to categorize greenness dynamics, reduces the fractions of greening and browning to 0.5% and 1.7%, respectively. Therefore, as with forests in the drought-affected region, the dominant greenness dynamic in forests outside is also one of no EVI changes. This conclusion is further re-enforced by nearly identical distributions of standardized anomalies between these two groups of forests (figure 3(c)). The peaks of these distributions differ trivially. These small differences actually show a slightly higher frequency of positive EVI anomalies amongst forests outside the drought-affected region (10%) than those within (8.5%), and a slightly higher frequency of negative EVI anomalies amongst forests within (10%) than outside (9%), which does not support the idea of a drought-induced greening response from these forests (Saleska *et al* 2007). The recurring theme from multiple analyses presented in this section is one of no widespread changes in the greenness of Amazonian forests south of the equator during the dry season of 2005.

4.2. Greenness dynamics during the 2000–9 decade

The proportion of the 2005 drought area with corrupted EVI data remains remarkably similar in all ten years of the 2000–9 period, about 66% (table 2)—this exemplifies the prevalence of clouds and aerosols selectively in some parts of the Amazon, year after year. Thus, the time series of uncorrupted EVI data required for unbiased estimation of anomalies is not available for pixels in these areas, even at the monthly scale (cf section 3.2.1). A predominant proportion of the forests, for which the complete set of uncorrupted data records is available, 56–77%, shows no discernible EVI changes. Comparable, albeit small, proportions of anomalous greening and browning are observed in six of the ten years, irrespective of the deficit in precipitation (years 2000–2, 2006–8). A slightly higher proportion of anomalous greening, relative to browning, is observed in drought (2005) as well as non-drought years (2003 and 2004). In 7 of the 9 non-drought years, the distributions of EVI anomalies display negative skew, similar to the distribution in the drought year 2005 (figure not shown for brevity)—patches of anomalous greening and browning, independent of the extent of precipitation deficit, are seen in many of these years as well. In contrast, the distribution of precipitation anomalies in 2005 exhibits positive skew (figure not shown for brevity)—nearly all the anomalies are negative. Interestingly, a significant browning anomaly is observed in 2009 (figure 4), but there was no correspondingly severe precipitation deficit (table 2). The quality flags also do not indicate anomalously enhanced atmospheric corruption in 2009. An inspection of the 2009 anomaly magnitudes reveals that nearly all the negative EVI anomalies are smaller than |0.04| in magnitude (figure 4), that is, less than the 2 std. dev. error bar of EVI (∼|0.06|), and therefore are statistically insignificant. Overall, these results fail to demonstrate a linkage between contemporaneous variations in dry season precipitation and greenness dynamics in this region. It is possible that these forests remain hydrated during the short dry season via their deep root systems (Wright *et al* 1996, Nepstad *et al* 1994) and/or through hydraulic redistribution (da Rocha *et al* 2004, Oliveira *et al* 2005). An extended period of drought has been reported to severely impact the forests and result

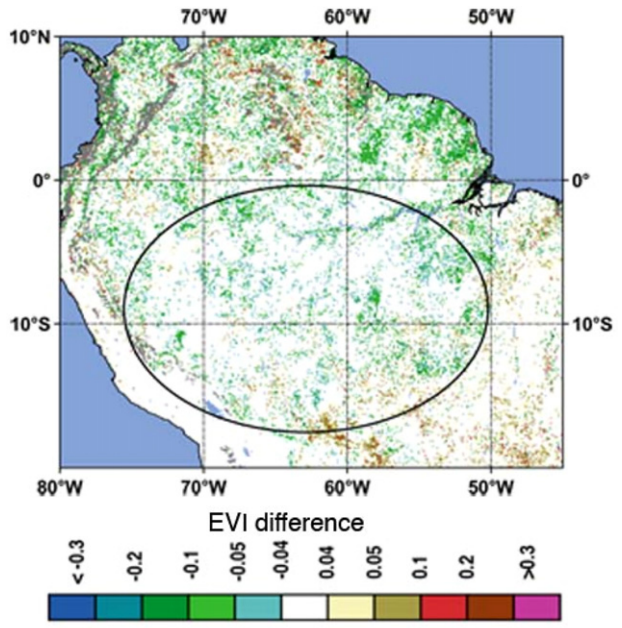

Figure 4. Spatial patterns of EVI anomalies during the 2009 dry season (July–September) at 1×1 km^2 spatial resolution. Cloud-, shadow-, climatology aerosol- and high aerosol-contaminated data are screened from analysis. Anomalies are calculated relative to 2000–8 using the methodology in section 3.2.2, and expressed as EVI differences.

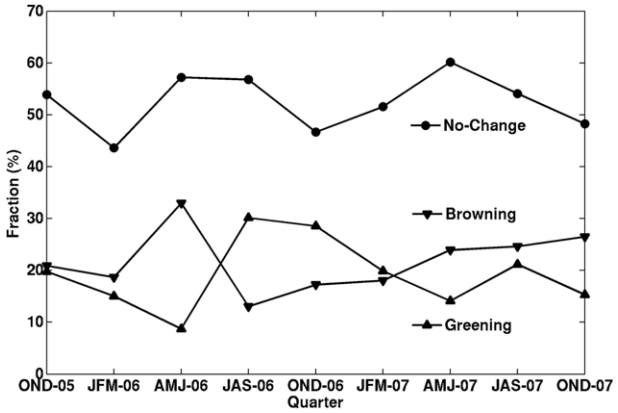

Figure 5. Fractions (%) of forests in the drought-affected area showing greening during the July to September quarter of 2005 that display greening, browning and no change from October–December (OND) quarter of 2005 through OND quarter of 2007. Pixels with EVI standardized anomalies in the range -1 to $+1$ std. dev. are classified as showing no changes. Pixels with EVI standardized anomalies less than -1 std. dev. are classified as browning. Pixels with EVI standardized anomalies greater than $+1$ std. dev. are classified as greening. Cloud, shadow, climatology aerosol and high aerosol-contaminated data are screened.

in mortality of large trees (Nepstad *et al* 2007). There are also reports of enhanced tree mortality and declines in tree growth in response to the 2005 drought (Phillips *et al* 2009)—possibly the moderate resolution (1×1 km^2) MODIS EVI data analyzed in this study fail to capture these changes, which were observed in several plots across the Amazon. In addition, the interpretation of greenness dynamics is further complicated by both man-made interferences such as logging (Koltunov *et al* 2009) and natural disturbances such as severe storms (Negron-Juárez *et al* 2010).

The gradual increase in EVI during the dry season (figure 1(a)) has been interpreted as indicative of leafing and enhanced photosynthetic activity (Huete *et al* 2006). Indeed, moist tropical forests are known to flush new leaves during the light rich dry season (van Schaik *et al* 1993, Wright and Vanschaik 1994, Myneni *et al* 2007). Leaf demography studies in tropical forests indicate leaf longevities of two to four years (Reich *et al* 2004). A recent study (Brando *et al* 2010) suggests that inter-annual variations in basin-wide (dry season) EVI are related to leaf flushing. Therefore, if the most extensive greening anomaly, seen in the drought year 2005 (0.26 million km^2), is suggestive of enhanced leaf area, and not an artifact, this anomaly should persist in to the following year(s)—discounting for the moment that the magnitudes of EVI anomalies in this region are statistically insignificant. Our analysis indicates no persistence of this greening anomaly, even in to the next quarter—random patches, some large and many small, of anomalous browning and greening appear in each quarter, with no distinct pattern of persistence (results not shown for brevity). A dominant proportion (50–60%) of the 2005 greening pixels show no anomalous EVI changes and comparable proportions, about 20%, show greening and browning in the following two years (figure 5)—thus, on an average, only 20% of the forests that displayed greening in 2005 maintained their enhanced greenness level through the following years. These results do not indicate enhanced leaf production as the cause of anomalous dry season greening in 2005.

5. Conclusions

The presence atmospheric contamination in satellite-derived greenness data over Amazon forests poses both temporal and spatial sampling issues. Removal of such data from the time series of observations can introduce large biases in the estimated means, standard deviations and anomalies. However, if such pixels, which lack the full complement of data, are dropped from analysis, the data available for analysis may be considerably reduced. For example, about 60–66% of the area affected by drought in 2005 lacks uncorrupted EVI data to unbiasedly estimate quarterly standardized anomalies. Given the selective prevalence of clouds and aerosols, the uncorrupted data are not representative of the larger drought area, and therefore, greenness dynamics inferred from the available sample cannot be extrapolated to the larger area.

A decade's worth of Terra MODIS collection 5 EVI data and six years of a previous version, both analyzed in multiple ways and taking into account EVI accuracy, consistently show a pattern of negligible changes in the greenness levels of forests both in the area affected by drought in 2005 and outside it. Small random patches of anomalous greening and browning—especially prominent in 2009—appear in all ten years, irrespective of contemporaneous variations in precipitation, but with no persistence over time. The fact that over 90% of the EVI anomalies are insignificantly

small—within 2 std. dev. (95% confidence interval) envelope of error in EVI—warrants cautious interpretation of these results: there were no changes in the greenness of these forests, or if there were changes, the EVI data failed to capture these either because the constituent reflectances were saturated or the moderate resolution precluded viewing small-scale variations.

This analysis demonstrates that there is a need to rigorously evaluate satellite-measured greenness data before utilizing in interpretation of vegetation greenness changes. In particular, atmospheric influences should be properly screened out, and any resulting biases should be well understood. Further, there is a need for more accurate and spatially resolved synoptic views from satellite data and corroborating comprehensive ground sampling to understand the greenness dynamics of Amazon forests.

Acknowledgment

This research was funded by the NASA Earth Science Enterprise.

Appendix

In this appendix, the biases in 2005 July to September quarterly mean EVI (x), climatological quarterly mean EVI (m), corresponding quarterly standard deviation (s) and standardized anomaly (a), calculated as $(x - m)/s$ are quantified. The biases are expressed relative to true x, m, s and a, which are evaluated from forest pixels in the 2005 drought-impacted region with complete uncorrupted 16-day EVI records during 2000–6 (6595 pixels) in collection 5 (C5) and 2000–5 (7385 pixels) in collection 4 (C4).

A.1. Type 1 bias

This type of bias is introduced in estimates of x, m, s and a, when filtering of corrupted data reduces the uncorrupted EVI record to less than three months in a quarter. One way of demonstrating this is to bias x, while keeping m and s unchanged, by shortening the data record as follows: one month (September, S) and from two months (August and September, AS) of data are dropped from analysis. The average of the remaining data ($x1$) is thus a biased estimate of x. The bias in $x(\Delta x)$ is $x1 - x$. Similarly, the standardized anomaly ($a1$), calculated as $(x1 - m)/s$, is a biased estimate of a, and the bias in a, denoted as Δa, is given by $a1 - a$.

Figure A.1 shows the distributions of Δx, which are positively skewed—average bias ($\overline{\Delta x}$) is negative ($p < 0.0001$)—across both collections. This effect is more pronounced in AS than in A. This shows that the average of 16-day EVI values from July (AS) or July and August (S) alone is an under-estimate of the quarterly mean because of EVI changes during this quarter (figure A.1(a)). This under-estimation increases as the number of months with missing data increases from one (S) to two (AS).

Biases in x generate biases in a, expressed as $|\Delta a|/|a|$ (table A.1). The biases are significant in magnitude—about three to four times—compared to the true standardized anomalies. The biases inflate as the length of EVI record is reduced from two (S) to one month (AS). These biases will generate spurious greenness changes. Eliminating them requires each month in a quarter to have at least one uncorrupted 16-day EVI value (cf section 3.2.1); pixels not satisfying this condition will not have third-quarter EVI mean in a given year(s), which results in another kind of bias as demonstrated next.

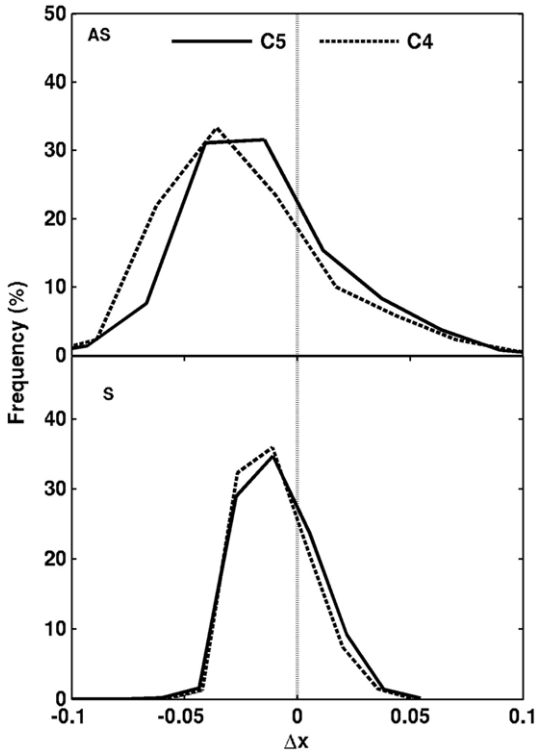

Figure A.1. Distribution of bias (Δx) in 2005 third-quarter mean EVI (1×1 km^2–collections 4 and 5) for cases S (no data in September) and AS (no data in August and September). The statistical significance of the average bias ($\overline{\Delta x}$), in each case, is determined using a t-test under the null hypothesis that $\overline{\Delta x}$ equals 0. The number of samples (pixels) is 6595 in C5 and 7385 in C4.

Table A.1. Percentiles of the magnitude of relative bias ($|\Delta a|/|a|$) in 2005 EVI standardized anomaly (1×1 km^2—collections 4 and 5) for cases S (no data in September) and AS (no data in August and September). The number of samples (pixels) is 6595 in C5 and 7385 in C4.

	S		AS	
Percentiles of $\|\Delta a\|/\|a\|$	C4	C5	C4	C5
25th	0.35	0.34	0.96	0.78
50th	0.82	0.70	1.76	1.30
75th	1.72	1.42	3.87	2.57

A.2. Type 2 bias

This type of bias is introduced in estimates on m and s, and therefore a, when third-quarter mean EVI is missing in one or more years. This is demonstrated by shortening the

Table A.2. Percentiles of the magnitude of relative bias ($|\Delta a|/|a|$) in 2005 standardized anomaly (1×1 km^2—collections 4 and 5) for third-quarter EVI data missing in 2004, 2003–4 and 2002–4. The number of samples (pixels) is 6595 in C5 and 7385 in C4.

	2004		2003–4		2002–4	
Percentiles of $\|\Delta a\|/\|a\|$	C4	C5	C4	C5	C4	C5
25th	0.12	0.09	0.20	0.19	0.34	0.56
50th	0.21	0.17	0.39	0.40	0.72	1.21
75th	0.60	0.23	1.22	0.55	2.51	1.60

reference period as follows: data are dropped from one year (2004), two years (2003–4) and three years (2002–4). These years are chosen for the sake of brevity—data can be dropped from other combinations of years too. In each of the three cases, the average of the remaining data ($m1$) is a biased estimate of m, while the standard deviation ($s1$) is a biased estimate of s. Thus, the standardized anomaly ($a1$), calculated as $(x - m1)/s1$, is a biased estimate of a, and therefore, bias in a, denoted as Δa, is given by $a1 - a$.

Percentiles of bias in a, expressed as $|\Delta a|/|a|$, are shown in table A.2. Biases inflate steadily—about 10% to over two and a half times (250%) relative to true estimates of standardized anomalies—as the number of years with missing data increases from one to three years. The increase in bias magnitude is due primarily to relatively large changes in estimate of quarterly standard deviation as more and more years are dropped (results not shown for brevity). Such biases will, therefore, generate greenness artifacts depending upon how many years lack third-quarter mean EVI. Elimination of these biases requires that each year of the reference period has a valid third-quarter mean EVI (cf section 3.2.1).

References

Aragao L, Malhi Y, Roman-Cuesta R M, Saatchi S, Anderson L O and Shimabukuro Y E 2007 Spatial patterns and fire response of recent Amazonian droughts *Geophys. Res. Lett.* **34** L07701

Aragao L *et al* 2009 Above- and below-ground net primary productivity across ten Amazonian forests on contrasting soils *Biogeosciences* **6** 2759–78

Brando P M, Goetz S J, Baccini A, Nepstad D C, Beck P S A and Christman M C 2010 Seasonal and interannual variability of climate and vegetation indices across the Amazon *Proc. Natl Acad. Sci. USA* **107** 14685–90

da Rocha H R, Goulden M L, Miller S D, Menton M C, Pinto L, de Freitas H C and Figueira A 2004 Seasonality of water and heat fluxes over a tropical forest in eastern Amazonia *Ecol. Appl.* **14** S22–32

Didan K and Huete A 2006 *MODIS Vegetation Index Product Series Collection 5 Change Summary* (http://modland.nascom.nasa.gov/QA_WWW/forPage/MOD13_VI_C5_Changes_Document_06_28_06.pdf)

Friedl M A, Sulla-Menashe D, Tan B, Schneider A, Ramankutty N, Sibley A and Huang X M 2010 MODIS collection 5 global land cover: algorithm refinements and characterization of new datasets *Remote Sens. Environ.* **114** 168–82

Huete A, Didan K, Miura T, Rodriguez E P, Gao X and Ferreira L G 2002 Overview of the radiometric and biophysical performance of the MODIS vegetation indices *Remote Sens. Environ.* **83** 195–213

Huete A R, Didan K, Shimabukuro Y E, Ratana P, Saleska S R, Hutyra L R, Yang W Z, Nemani R R and Myneni R 2006 Amazon rainforests green-up with sunlight in dry season *Geophys. Res. Lett.* **33** L06405

Justice C O *et al* 1998 The moderate resolution imaging spectroradiometer (MODIS): land remote sensing for global change research *IEEE Trans. Geosci. Remote Sens.* **36** 1228–49

Koltunov A, Ustin S L, Asner G P and Fung I 2009 Selective logging changes forest phenology in the Brazilian Amazon: evidence from MODIS images time series analysis *Remote Sens. Environ.* **113** 2431–40

Malhi Y and Grace J 2000 Tropical forests and atmospheric carbon dioxide *Trends Ecol. Evolut.* **15** 332–7

McGuffie K, Hendersonsellers A, Zhang H, Durbridge T B and Pitman A J 1995 Global climate sensitivity to tropical deforestation *Glob. Planet. Change* **10** 97–128

Myneni R B *et al* 2007 Large seasonal swings in leaf area of Amazon rainforests *Proc. Natl Acad. Sci. USA* **104** 4820–3

Negron-Juárez R I *et al* 2010 Widespread Amazon forest tree mortality from a single cross-basin squall line event *Geophys. Res. Lett.* **37** L16701

Nepstad D C, Decarvalho C R, Davidson E A, Jipp P H, Lefebvre P A, Negreiros G H, Dasilva E D, Stone T A, Trumbore S E and Vieira S 1994 The role of deep roots in the hydrological and carbon cycles of Amazonian forests and pastures *Nature* **372** 666–9

Nepstad D C, Tohver I M, Ray D, Moutinho P and Cardinot G 2007 Mortality of large trees and lianas following experimental drought in an amazon forest *Ecology* **88** 2259–69

Oliveira R S, Dawson T E, Burgess S S O and Nepstad D C 2005 Hydraulic redistribution in three Amazonian trees *Oecologia* **145** 354–63

Phillips O L, Hall P, Gentry A H, Sawyer S A and Vasquez R 1994 Dynamics and species richness of tropical rain-forests *Proc. Natl Acad. Sci. USA* **91** 2805–9

Phillips O L *et al* 2009 Drought sensitivity of the Amazon rainforest *Science* **323** 1344–7

Rahman A F, Sims D A, Cordova V D and El-Masri B Z 2005 Potential of MODIS EVI and surface temperature for directly estimating per-pixel ecosystem C fluxes *Geophys. Res. Lett.* **32** L19404

Reich P B, Uhl C, Walters M B, Prugh L and Ellsworth D S 2004 Leaf demography and phenology in Amazonian rain forest: a census of 40 000 leaves of 23 tree species *Ecol. Monographs* **74** 3–23

Saleska S R, Didan K, Huete A R and da Rocha H R 2007 Amazon forests green-up during 2005 drought *Science* **318** 612

Samanta A, Ganguly S and Myneni R B 2011a MODIS enhanced vegetation index data do not show greening of Amazon forests during the 2005 drought *New Phytol.* **189** 12–5

Samanta A *et al* 2010 Amazon forests did not green-up during the 2005 drought *Geophys. Res. Lett.* **37** L05401

Samanta A *et al* 2011b Comment on 'Drought-induced reduction in global terrestrial net primary production from 2000 through 2009' *Science* **333** 6046

Samanta A *et al* 2012 Seasonal changes in leaf area of Amazon forests from leaf flushing and abscission *J. Geophys. Res* **117** G01015

Sims D A *et al* 2008 A new model of gross primary productivity for North American ecosystems based solely on the enhanced vegetation index and land surface temperature from MODIS *Remote Sens. Environ.* **112** 1633–46

Sombroek W 2001 Spatial and temporal patterns of Amazon rainfall—consequences for the planning of agricultural occupation and the protection of primary forests *Ambio* **30** 388–96

ter Steege H *et al* 2006 Continental-scale patterns of canopy tree composition and function across Amazonia *Nature* **443** 444–7
van Schaik C P, Terborgh J W and Wright S J 1993 The phenology of tropical forests—adaptive significance and consequences for primary consumers *Ann. Rev. Ecol. Systematics* **24** 353–77
Vermote E F, El Saleous N Z and Justice C O 2002 Atmospheric correction of MODIS data in the visible to middle infrared: first results *Remote Sens. Environ.* **83** 97–111
Vermote E F and Kotchenova S 2008 Atmospheric correction for the monitoring of land surfaces *J. Geophys. Res.* **113** D23S90
Vermote E F and Vermuelen A 1999 *Atmospheric Correction Algorithm: Spectral Reflectances (MOD09) MODIS Algorithm Theoretical Basis Document* (http://modis.gsfc.nasa.gov/data/atbd/atbd_mod08.pdf)
Werth D and Avissar R 2002 The local and global effects of Amazon deforestation *J. Geophys. Res. Atmos.* **107** D20
Wright S J and Vanschaik C P 1994 Light and the phenology of tropical trees *Am. Natural.* **143** 192–9
Wright S J 1996 Phenological responses to seasonality in tropical forest plants *Tropical Forest Plant Ecophysiol* ed S S Mulkey, R L Chazdon and A P Smith (New York: Chapman and Hall) pp 440–60
WWW1 2011 NASA Land Processes Data Active Archive Center (LP DAAC), MOD13A2 (https://lpdaac.usgs.gov/content/view/full/6648)
WWW2 2011 NASA Land Processes Data Active Archive Center (LP DAAC), MOD13C2 (https://lpdaac.usgs.gov/content/view/full/6665)
WWW3 2011 NASA Land Processes Data Active Archive Center (LP DAAC), MOD12Q1 (https://lpdaac.usgs.gov/lpdaac/products/modis_products_table/land_cover/yearly_l3_global_1km2/mod12q1)
WWW4 2011 Goddard Earth Sciences Data and Information Services Center, TRMM 3B43 (http://disc.sci.gsfc.nasa.gov/precipitation/documentation/TRMM_README/TRMM_3B43_readme.shtml)
WWW5 2011 Product quality documentation for MOD13A2, C5 (http://landweb.nascom.nasa.gov/cgi-bin/QA_WWW/detailInfo.cgi?prod_id=MOD13A2&ver=C5)
WWW6 2011 MODIS Land Surface Reflectance Science Computing Facility (http://modis-sr.ltdri.org/validation/accuracy_uncertainty.html)
Xiao X M, Hagen S, Zhang Q Y, Keller M and Moore B 2006 Detecting leaf phenology of seasonally moist tropical forests in South America with multi-temporal MODIS images *Remote Sens. Environ.* **103** 465–73
Xu L *et al* 2011 Widespread decline in greenness of Amazonian vegetation due to the 2010 drought *Geophys. Res. Lett.* **38** L07402
Zhao M S and Running S W 2010 Drought-induced reduction in global terrestrial net primary production from 2000 through 2009 *Science* **329** 940